Journal of Earth Science, *Vol. 34*, *No. 6*, *p. 1704−1716*, *December 2023* *ISSN 1674-487X*
Printed in China
https://doi.org/10.1007/s12583-020-1111-6

Permian-Triassic Magmatism in the Qin-Fang Tectonic Belt, SW China: New Insights into Tectonic Evolution of the Eastern Paleo-Tethys

Yun Zhou[1], **Yongshan Zhao**[1], **Yongfeng Cai**[*1], **Qiaofan Hu**[2], **Ce Wang**[3]
1. *Collaborative Innovation Center for Exploration of Nonferrous Metal Deposits and Efficient Utilization of Resources*, *Guangxi Key Laboratory of Hidden Metallic Ore Deposits Exploration*, *Guilin University of Technology*, *Guilin* 541004, *China*
2. *China Nonferrous Metals* (*Guilin*) *Geology and Mining Co.*, *Ltd.*, *Guilin* 541004, *China*
3. *School of Marine Sciences*, *Sun Yat-sen University*, *Zhuhai* 519082, *China*
Yun Zhou: https://orcid.org/0000-0001-9688-6659; Yongfeng Cai: https://orcid.org/0000-0002-0110-1335

ABSTRACT: The granites of ambiguous geodynamic mechanism in the Qin-Fang tectonic belt (SW China) were studied in detail based on petrological, element geochemical, zircon U-Pb geochronological, and Hf isotopic data. LA-ICPMS U-Pb analyses on zircon yield ages of 248–245 Ma for the granites from the Qin-Fang tectonic belt. The geochemical data show that they are high-K, calc-alkaline, and peraluminous series. Their $\varepsilon_{Hf}(t)$ values are from -14.01 to -7.75 with two-stage model ages of 1.74–1.43 Ga. These data, integrated with low Al_2O_3/TiO_2, Rb/Sr, Rb/Ba, and $(Na_2O + K_2O)/(FeO^T + MgO + TiO_2)$ ratios, and high CaO/Na_2O ratios for the granite, suggest an origin from psammite source which was contaminated by mantle-derived components. These observations, in combination with the age data and stratigraphic records in the Jinshajiang, Ailaoshan, and Hainan Island areas suggest that the granites were formed in a post-collision tectonic setting. The Qin-Fang tectonic belt was likely a branched ocean basin of the eastern Paleo-Tethys.
KEY WORDS: Paleo-Tethyan ocean, zircon, granite, Permian-Triassic, Qin-Fang tectonic belt.

0 INTRODCTION

The Paleo-Tethyan Ocean is originally regarded as a Paleozoic ocean basin situated between the Laurasia and Gondwana continents (Allen et al., 2023; Metcalfe, 1996; Şengör, 1979). The eastern Paleo-Tethyan tectonic belts are well recorded in Southeast Asia, e.g., SW China, NW Vietnam and northern Laos (Liu et al., 2023; Qiu et al., 2021; Qian et al., 2019; Shi et al., 2019; Yang et al., 2019; Zhai et al., 2019; Sone and Metcalfe, 2008). The Sanjiang tectonic belt, one of the most important eastern Paleo-Tethyan tectonic belt in Yunnan Province, SW China, contains several micro-continental blocks (e. g., Tengchong, Baoshan-Sibumasu and Simao-Indochina blocks) and multiple plate suture zones (e. g., the Nujiang, the Changning-Menglian and the Jinshajiang-Ailaoshan suture zones). These suture zones are composed of a set of Permian–Triassic igneous rocks (including ophiolites or ophiolitic mélanges, and island-arc volcanic rocks; Liu et al., 2023; Yin et al., 2023; Zhai et al., 2019; He et al., 2018; Peng et al., 2013; Zi et al., 2012; Jian et al., 2009), high-pressure metamorphic rocks (e. g., eclogite and blueschist; Wang et al., 2019; Fan et al., 2015) and sedimentary rocks (Zhong, 1998). The Changning-Menglian suture zone extends into Thailand to the south and is considered as the position of the main ocean basin (Zhong, 1998). The Jinshajiang-Ailaoshan suture zone extends into NW Vietnam to the southeast and is generally viewed as a branch of the Paleo-Tethyan Ocean (Liu et al., 2015). However, whether there is a branched ocean basin at further northeast part of the eastern Paleo-Tethys is still unclear.

The Qin-Fang tectonic belt in SW Guangxi Zhuang Autonomous Region, South China, tectonically is located at the junction of the Indochina, Yangtze and Cathaysia blocks. It is also located at the transitional area between the Paleo-Tethyan and the Paleo-Pacific tectonic domains. Such a special tectonic position makes the tectonic belt to be an ideal region to probe into the tectonic evolution between the South China and the Indochina blocks. Extensive Permian – Triassic granites intruded into the Qin-Fang tectonic belt that constitutes a well-known S-type granite belt named Darongshan granite complex (Xu et al., 2018; Li et al., 2016; Jiao et al., 2015; Zhao et al., 2012; Chen et al., 2011; Charoy and Barbey, 2008). However, their formation age is still debatable with Late Permian age of 275–253 Ma (Charoy and Barbey, 2008) or Early Triassic age of 251 – 248 Ma (Jiao et al., 2015), and their geodynamic mechanism is also controversial. Deng et al. (2004) suggested that the Darongshan granites were derived from anatexis of ancient crust due to crustal thickening in intracontinental environment. Chen et al. (2011) proposed a tectonic model of double subduction be-

*Corresponding author: caiyongfeng@glut.edu.cn

Manuscript received August 15, 2020.
Manuscript accepted October 20, 2020.

Zhou Yun, Zhao Yongshan, Cai Yongfeng, Hu Qiaofan, Wang Ce, 2023. Permian-Triassic Magmatism in the Qin-Fang Tectonic Belt, SW China: New Insights into Tectonic Evolution of the Eastern Paleo-Tethys. *Journal of Earth Science*, 34(6): 1704–1716. https://doi.org/10.1007/s12583-020-1111-6. http://en.earth-science.net

tween the South China and Indochina blocks triggered by mantle plume to explain the formation of the Darongshan granites. Qin et al. (2013) argued that the generation of the Darongshan granites is related to oceanic crust subduction between the Yangtze and Cathaysia blocks. Jiao et al. (2015) held the view that the Darongshan granites were generated in a back-arc basin and contemporaneous basalts were produced by slab rollback and tearing in the period of Permian–Triassic. Xu et al. (2018) interpreted that the Darongshan granites together with the mantle-derived mafic rocks were produced by oblique subduction of the Paleo-Pacific Plate beneath South China.

In this paper, we present detailed petrological, whole-rock geochemical, zircon U-Pb geochronological and *in situ* Hf isotopic study on the Darongshan granites along the Qin-Fang tectonic belt. Our aims are to constrain the petrogenesis of the Permian-Triassic granites in the Qin-Fang tectonic belt, and further to decipher their possible geodynamic mechanism.

1 GEOLOGICAL BACKGROUND AND SAMPLES

The South China Block is composed of the Yangtze and Cathaysia blocks, which were generally considered to be combined along the Jiangnan (Sibao) orogenic belt in the Neoproterozoic (Ma et al., 2021; Cai et al., 2020, 2014; Zhao and Cawood, 2012). The Qin-Fang tectonic belt is located at the junctional part of the Yangtze and Cathaysia blocks. It is separated from the Yunkai massif (SW Cathaysia Block) to the east by the Bobai-Cenxi fault, and is bounded to the Shiwandashan Basin to the west by the Fulong-Xiaodong fault (Fig. 1). The northwestern margin of the Shiwandashan Basin is separated from the Devonian – Middle Triassic Youjiang Basin by the Pingxiang-Nanning fault (Fig. 1).

Strata within the Qin-Fang tectonic belt are mainly Silurian to Cretaceous. The Silurian to Permian strata are principally exposed in the eastern and southern parts of the belt. The Triassic to Cretaceous strata are mainly distributed in the western and northern parts of the belt (Fig. 1; Zhao et al., 2023). The Silurian slight metamorphic succession with the largest sedimentary thickness of >7 000 m is mainly composed of sandstone, siltstone, sandy shale, and phyllitic shale, and shows the character of flyschoid sequence. It can be further divided into, from base to top, Liantan Group, Wentoushan Group and Fangcheng Group. The Devonian strata are in conformable contact with the underlying Silurian, and can be divided into Qinzhou Group, Xiaodong Group and Liujiang Group. The Qinzhou and Liujiang groups mainly consist of siliceous rock, argillaceous siliceous rock, and siltstone. The Xiaodong Group is mainly composed of, from bottom to top, conglomerate, fine sandstone, siltstone, sandy mudstone, and carbon mudstone. It is in unconformable relation with the underlying Qinzhou Group. Carboniferous strata are commonly missing in the region. The Permian strata are mainly made up of conglomerate, fine sandstone, siltstone, argillaceous siltstone, mudstone, and silty mudstone. The Lower Triassic strata primarily consist of fine sandstone, mudstone, and interstratified pebbly sandstone and siltstone. They are in unconformable contact with the overlying Upper Triassic strata which mainly consist of granitic conglomerate, pebbly sandstone, medium-coarse grained sandstone, argillaceous siltstone, and fine sandstone. The Jurassic strata are primarily composed of fine sandstone, argillaceous siltstone, silty mudstone, and quartz sandstone. The Cretaceous strata are in unconformable contact with the underlying Jurassic strata, and mainly contain calcareous siltstone, sandstone, siltstone, mudstone, conglomerate, breccia, and andesite.

The Darongshan granite complex covers a total area of > 10 000 km^2 and outcrops mainly in the Silurian-Cretaceous strata. It contains Darongshan, Pubei, Jiuzhou, and Taima plu-

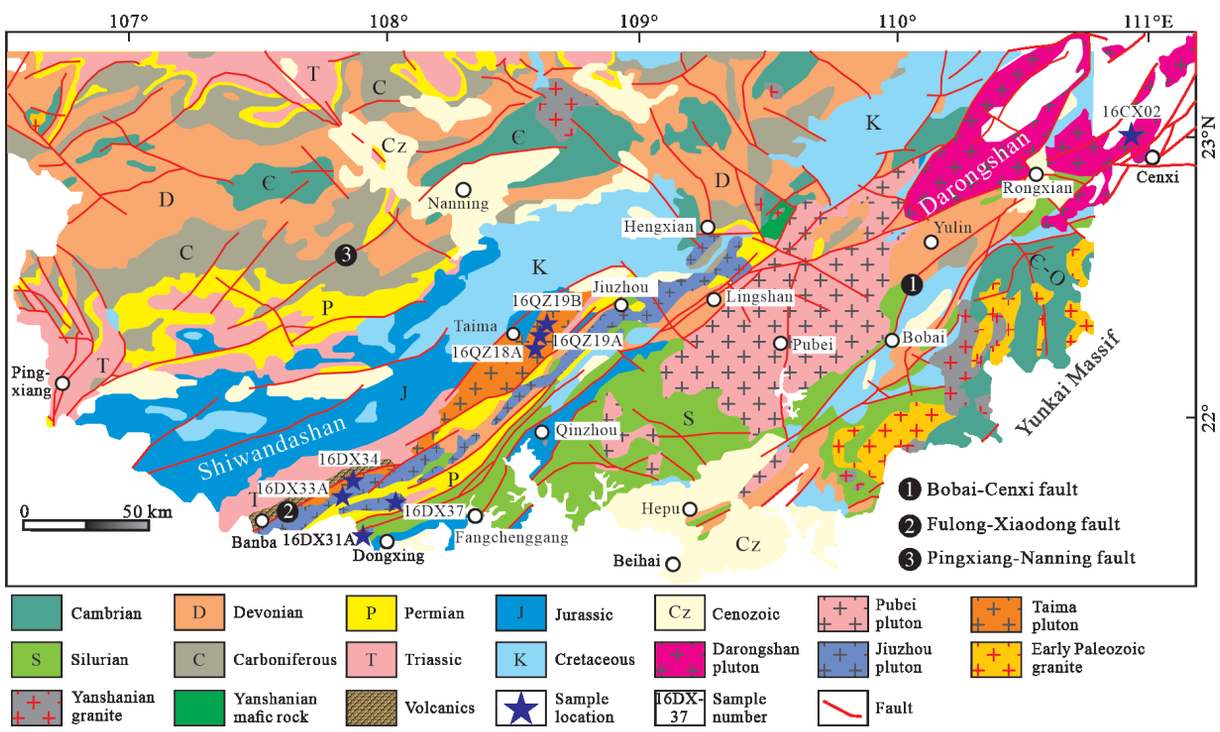

Figure 1. Schematic geotectonic framework showing the Qin-Fang tectonic belt and its surrounding areas.

tons. The Darongshan and Pubei plutons show similar lithology, and are mainly composed of cordierite-biotite granite. The Jiuzhou pluton comprises primarily of cordierite-, biotite- and hypersthene-bearing monzogranite. The outer and inner phases of the pluton are fine-grained and coarse-grained, respectively. An important feature of the Jiuzhou pluton is that it contains numerous enclaves which consist principally of metapelitic granulite and quartzo-feldspathic gneiss (>90%), and a few metasandstone, hornfels, and quartzite. The Taima pluton is made up of orthopyroxene-bearing granite porphyry. Additionally, a set of Triassic volcanic rocks are exposed in the west of the Taima pluton. These volcanic rocks are mainly composed of rhyolite, perlite, and tuffolava. Recently, Xu et al. (2018) have reported that Late Permian–Early Triassic (250–248 Ma, LA-ICP-MS zircon U-Pb age) dolerite intrudes as stocks into the Proterozoic or Ordovician-Silurian strata at the northeast Darongshan pluton.

Sample 16CX02 (22°58′16″N, 110°53′38.7″E), collected from the Darongshan pluton, is medium- to fine-grained cordierite-biotite granite, and has a porphyaceous texture and a massive structure (Fig. 2a). It is made up of quartz (35%–40%), plagioclase (25%–30%), K-feldspar (20%–25%), biotite (5%–10%), and minor cordierite. The accessory minerals include zircon, ilmenite, apatite, monazite, chlorite, and tourmaline (Fig. 2b). The quartz is mostly anhedral with size in range of 0.2–2 mm and some of them show melting corrosion structure (Fig. 2b). The plagioclase occurs as subhedral crystals with grain size of 1–3 mm and some of them are altered into kaolinite. The K-feldspar phenocrysts are subhedral and have grain size of 1–5 mm. The biotite is mostly brown and laminar, and shows different degrees of bending (Fig. 2b). The cordierite is anhedral with grain size of 0.5–2 mm and some of them are altered into sericite and muscovite.

Samples taken from the Taima pluton, 16QZ18A (22°19′0.1″N, 108°36′30.5″E), 16QZ19A (22°20′0″N, 108°36′16″E), 16QZ19B (22°20′0″N, 108°36′16″E), and 16DX34 (21°44′26.6″N, 107°47′35.7″E), are orthopyroxene-bearing granite porphyry, and have a porphyritic texture and a massive structure (Figs. 2c and 2e). The phenocrysts are subangular, round or corrosional, and are mainly composed of K-feldspar (35%–40%), quartz (30%–35%), plagioclase (10%–15%), and orthopyroxene (5%–10%). The matrixes are composed of felsic minerals and minor dark minerals (Figs. 2d and 2f).

Samples collected from the Jiuzhou pluton, 16DX31A (21°36′12.5″N, 107°54′43.4″E), 16DX33A (21°41′57.7″N, 107°48′6.1″E) and 16DX37 (21°40′9.4″N, 107°51′5.3″E), are characterized by hypersthene-, cordierite- and biotite-bearing monzogranite. They exhibit a porphyaceous texture and a massive structure (Fig. 2g), and consist of plagioclase (25%–30%), K-feldspar (25%–30%), quartz (20%–25%), biotite (10%–15%), and minor hypersthene and cordierite. The accessory minerals include zircon, ilmenite, apatite, chlorite, and secondary muscovite (Fig. 2h). The plagioclase occurs as subhedral crystals with grain size of 0.5–4 mm. The K-feldspar phenocrysts are mostly anhedral with grain size of 0.5–3 mm, and exhibit a perthitic structure in the core. The quartz is anhedral with size in range of 0.1–1 mm. The biotite is largely brown and laminar and always exhibits different degrees of bending (Fig. 2h). The hypersthene, usually associated with biotite, occurs as subhedral crystal with zircon and ilmenite as inclusions. The anhedral cordierite is prismatic with grain size of 0.2–1 mm and generally contains zircon, apatite and ilmenite as inclusions (Fig. 2h).

2 RESULTS

The LA-ICP-MS zircon U-Pb analyses were carried out on eight samples (16CX02, 16QZ18A, 16QZ19A, 16QZ19B, 16DX34, 16DX31A, 16DX33A and 16DX37) from the Darongshan granite complex, and the analysis results are shown in Table S1. Zircon grains sorted from these samples are mainly 100–300 μm long with aspect ratios of 1.5 : 1–2.5 : 1 and exhibit euhedral prismatic shapes with concentric zonation patterns in the CL images (Fig. S1). This suggests that they have a magmatic origin. Samples 16CX02 and 16QZ19A were chosen to perform in-situ zircon Hf isotopic compositions, and the results are shown in Table 1. Major oxide and trace element compositions were conducted, and the results are shown in Table 2. The detailed analytical methods are appended in the ESM.

2.1 Zircon U-Pb Geochronology and Hf Isotopic Results

Darongshan pluton: Twenty zircon grains from sample 16CX02 were analyzed. These zircons have Th/U ratios ranging from 0.10 to 0.42 (Table S1). Nine zircon grains yielded a $^{206}Pb/^{238}U$ weighted mean age of 246 ± 2 Ma, which is interpreted to be the crystallization age (Fig. 3). Four of the spots have $^{206}Pb/^{238}U$ ages of 941, 937, 838, and 829 Ma, and three have $^{207}Pb/^{206}Pb$ ages of 2 432, 2 322, and 1 529 Ma. These zircon grains are mostly andedral, and thus, they are inferred to be captured zircons from the wall rock or inherited zircons from the underlying basement. Some of the analyses are discordant, which is indicative of Pb loss due to later tectonothermal event(s).

Ten analyses on the sample 16CX02 yield $^{176}Lu/^{177}Hf$ ratios ranging from 0.000 416 to 0.001 478 and present-day $^{176}Hf/^{177}Hf$ ratios from 0.281 745 to 0.282 350 with initial $^{176}Hf/^{177}Hf$ ratios in range of 0.281 732–0.282 345. Their $\varepsilon_{Hf}(t)$ (t is the formation age of ca. 246 Ma) values range from -14.01 to -9.69 with two-stage model ages (T_{DM2}) from 1.74 to 1.52 Ga (Table 1).

Taima pluton: A total of eighty zircon grains from four samples (16QZ18A, 16QZ19A, 16QZ19B, 16DX34) of Taima pluton are analyzed. The four samples have Th/U ratios of 0.19–0.51, 0.11–0.63, 0.10–0.83, and 0.13–0.47, respectively (Table S1), and yield $^{206}Pb/^{238}U$ weighted mean ages of 247 ± 6 (N = 16), 246 ± 5 (N = 16), 246 ± 3 (N = 17), and 246 ± 6 Ma (N = 14), respectively (Figs. 3b–3e). This indicates that these samples have similar crystallization ages (ca. 246 Ma) within the measurement uncertainties. Some zircon grains have U-Pb ages of 2 284–731 Ma which are inferred to be captured zircons from the wall rock or inherited zircons from the underlying basement. One zircon grain yields a $^{207}Pb/^{206}Pb$ age of 3 539 ± 17 Ma (Table S1). This is the oldest known zircon age so far in igneous rocks from the Qin-Fang tectonic belt. Other analyses are discordant, which is indicative of Pb loss due to later tectonothermal event(s).

Ten analyses on zircons from the sample 16QZ19A have $^{176}Lu/^{177}Hf$ and present-day $^{176}Hf/^{177}Hf$ ratios in the range of

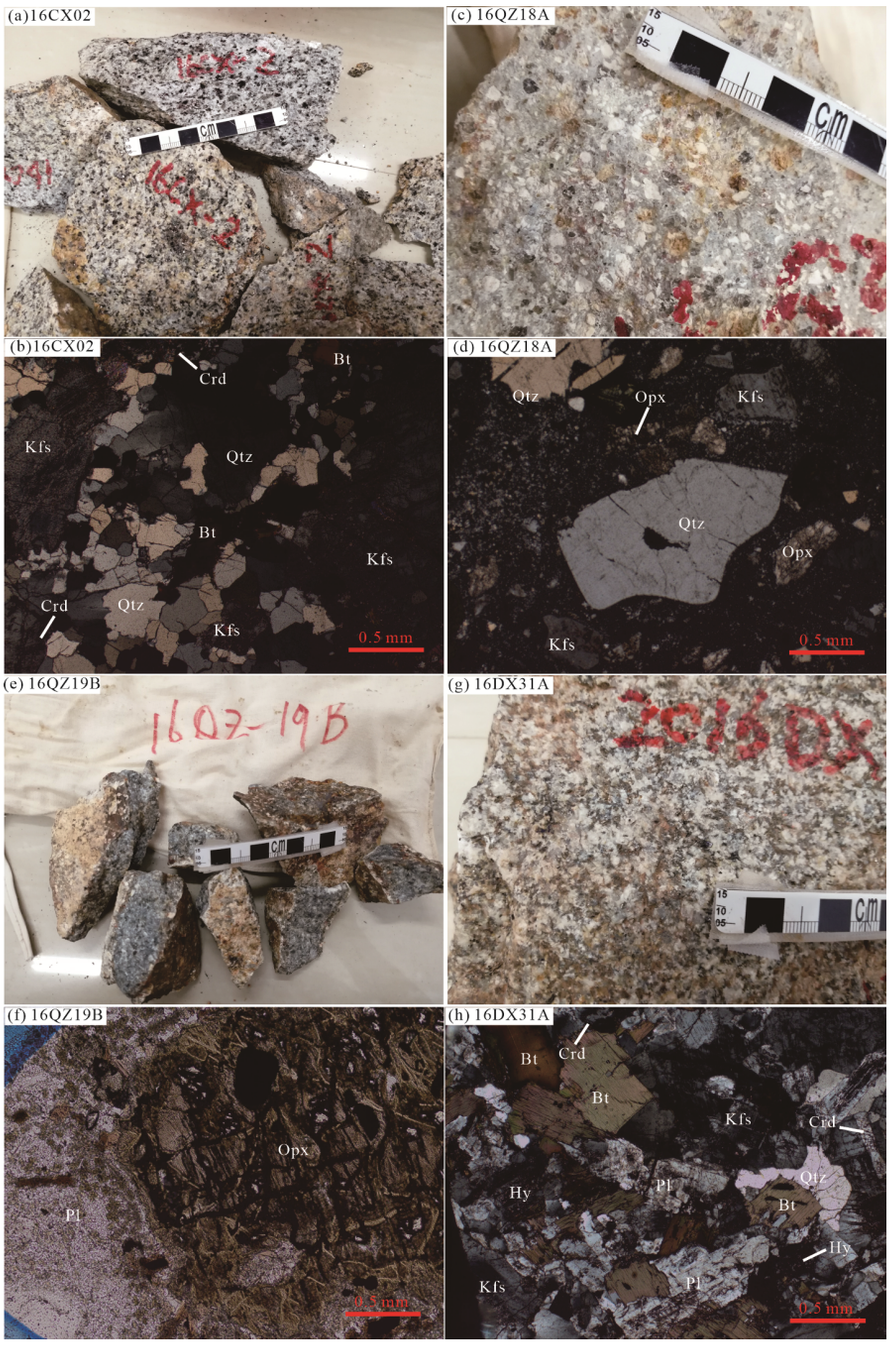

Figure 2. Field and microscope photographs for the granite from the Qin-Fang tectonic belt. Bt. Biotite; Kfs. K-feldspar; Crd. cordierite; Opx. orthopyroxene; Hy. hypersthene; Pl. plagioclase; Qtz. quartz.

0.000 973–0.002 155 and 0.281 969–0.282 407, respectively. Their initial $^{176}Hf/^{177}Hf$ ratios range from 0.281 926 to 0.282 400, and $\varepsilon_{Hf}(t)$ values from -12.35 to -7.75 with T_{DM2} of 1.66–1.43 Ga (Table 1).

Jiuzhou pluton: Seventy zircon grains in total from three samples (16DX31A, 16DX33A, 16DX37) of Jiuzhou pluton were analyzed. They mainly have Th/U ratios of 0.34–0.54, 0.10–0.60, and 0.13–0.63 (Table S1), and yield $^{206}Pb/^{238}U$ weighted mean ages of 248 ± 5 (N = 17), 245 ± 4 (N = 23), and 247 ± 5 Ma (N = 16), respectively (Figs. 3f–3h). This indicates that they have similar crystallization ages (ca. 246 Ma) within the measurement uncertainties. Some of the zircon grains have U-Pb ages of 2 287–792 Ma which are inferred to be captured zircons from the wall rock or inherited zircons from the underlying basement. Other fractions are discordant, which is indicative of Pb loss due to later tectonothermal event(s).

2.2 Geochemical Characteristics

Granites from the Darongshan granite complex have 70.75 wt.%–75.91 wt.% SiO_2 (Fig. 4), 12.20 wt.%–14.42 wt.% Al_2O_3, 0.63 wt.%–2.46 wt.% CaO, 0.18 wt.%–1.43 wt.% MgO, 1.25 wt.%–4.06 wt.% $Fe_2O_3^T$, 0.06 wt.%–0.19 wt.% P_2O_5, and 0.19 wt.%–0.58 wt.% TiO_2 (Fig. S2). They have total alkali (K_2O + Na_2O) of 5.93 wt.%–8.00 wt.% and K_2O/Na_2O ratios greater

Table 1 Analyzed results of zircon *in-situ* Hf isotopic compositions for the granite from the Qin-Fang tectonic belt

Spot No.	*t* (Ma)	$^{176}Yb/^{177}Hf$	$^{176}Lu/^{177}Hf$	$^{176}Hf/^{177}Hf$	2s	$^{176}Hf/^{177}Hf(i)$	$\varepsilon_{Hf}(t)$	2s	T_{DM1} (Ma)	T_{DM2} (Ma)
16CX02, Darongshan pluton										
1	246	0.045 959	0.001 478	0.282 277	0.000 012	0.282 270	-12.35	0.4	1 394	1 659
4	246	0.036 133	0.001 100	0.282 292	0.000 015	0.282 287	-11.76	0.5	1 360	1 631
8	246	0.028 182	0.000 923	0.282 328	0.000 015	0.282 324	-10.46	0.5	1 303	1 567
9	246	0.032 669	0.001 046	0.282 350	0.000 013	0.282 345	-9.69	0.4	1 276	1 529
12	246	0.037 725	0.001 218	0.282 229	0.000 013	0.282 223	-14.01	0.4	1 452	1 741
13	246	0.021 630	0.000 684	0.282 324	0.000 013	0.282 321	-10.56	0.5	1 300	1 572
7	484	0.015 142	0.000 516	0.282 197	0.000 013	0.282 193	-9.85	0.4	1 470	1 734
11	838	0.017 732	0.000 650	0.282 174	0.000 012	0.282 164	-3.01	0.4	1 506	1 690
3	941	0.030 829	0.000 964	0.282 175	0.000 013	0.282 158	-0.92	0.4	1 518	1 672
5	1 712	0.012 889	0.000 416	0.281 745	0.000 018	0.281 732	1.31	0.6	2 083	2 197
16QZ19A, Taima pluton										
1	246	0.032 145	0.001 146	0.282 360	0.000 012	0.282 354	-9.37	0.4	1 266	1 514
2	246	0.033 487	0.001 301	0.282 328	0.000 015	0.282 322	-10.52	0.5	1 316	1 570
3	246	0.034 224	0.001 212	0.282 397	0.000 014	0.282 392	-8.05	0.5	1 216	1 449
4	246	0.043 583	0.001 527	0.282 407	0.000 013	0.282 400	-7.75	0.4	1 212	1 434
6	246	0.026 713	0.000 973	0.282 285	0.000 014	0.282 281	-11.99	0.5	1 365	1 642
9	246	0.031 039	0.001 190	0.282 276	0.000 015	0.282 270	-12.35	0.5	1 386	1 659
11	246	0.049 242	0.001 754	0.282 330	0.000 016	0.282 322	-10.51	0.6	1 329	1 569
12	246	0.046 631	0.001 789	0.282 381	0.000 013	0.282 373	-8.72	0.5	1 258	1 481
13	246	0.049 364	0.001 674	0.282 310	0.000 013	0.282 302	-11.22	0.5	1 355	1 604
5	1 055	0.063 595	0.002 155	0.281 969	0.000 014	0.281 926	-6.59	0.5	1 862	2 046

than 1 (K_2O/Na_2O = 1.75–2.47). This suggests that they belong to the high-K calc-alkaline series (Fig. 4b). The molecular A/CNK [$Al_2O_3/(CaO + Na_2O + K_2O)$] and A/NK [$Al_2O_3/(Na_2O + K_2O)$] ratios of the samples are 1.06–1.27 and 1.24–1.74, respectively, pointing to a peraluminous composition (Fig. 4c).

The multi-element primitive mantle-normalized diagrams are characterized by depleted high field strength element (HFSE; e.g., Nb, Ta, Th, Hf, and Zr) and are enriched in large ion lithophile element (LILE; e. g., Rb, U, and K) (Fig. 5a). They exhibit negative anomalies in Nb, Ta, Ba, Sr, P and Ti (Fig. 5a). Rare earth element (REE) patterns exhibit an obvious negative slope from light rare earth element (LREE) to heavy rare earth element (HREE) with $(La/Yb)_{cn}$ = 3.88–14.28 (average of 7.38) (Fig. 5b). They also have higher fractionated LREE ($[La/Sm]_{cn}$ = 2.90–4.04; mean = 3.52) than HREE ([Gd/Yb]cn = 0.97–2.58; mean = 1.48). They are characterized by negative Eu anomalies with Eu* of 0.14–0.56 (mean = 0.44; Eu* = $[Eu/Sqrt (Sm \times Gd)]_{cn}$) (Fig. 5b).

3 DISCUSSION

3.1 Petrogenesis of the Granite

The granite samples from the Darongshan granite complex contain cordierite (Figs. 2b and 2h) and show high A/CNK values ranging from 1.06 to 1.27 (mean = 1.13; Fig. 4c). These geochemical features suggest that they are strongly peraluminous and are similar to those of S-type granite (Championa and Bultitude, 2013; Chappell and White, 1974). Studies of experimental petrology have revealed that massive peraluminous felsic melts are mainly produced by melting of crustal materials, such as greywacke, orthogneiss, metapelite, and amphibolite (Chappell and Wyborn, 2012). Most of the granite samples have lower Al_2O_3/TiO_2 ratios (23–43; average of 29), Rb concentrations (210 ppm–392 ppm; mean = 283 ppm), and higher CaO/Na_2O ratios (0.27–1.05; average of 0.74) (Fig. 6a; Table 2) than those of pelite-derived melts (Sylvester, 1998) indicating that their formation is not only derived from partial melting of a pure pelite. Additionally, studies of experimental petrology have also evinced that strongly peraluminous magma cannot be produced purely from partial melting of pelitic sediments (Kalsbeek et al., 2001; Miller, 1985). Thus, a pure pelite-dominated source for the Darongshan granite can be excluded.

Studies of experimental petrology have shown that peraluminous magma can be derived from dehydration melting of metaluminous basic metaigneous rock (e.g., amphibolite) at the lower crustal level (Kamei, 2002; Patiño Douce and Beard, 1995). Magma produced in this way dominatingly forms peraluminous intermediate rocks instead of strongly peraluminous rocks. Melting of high-grade metamorphic rocks in water sufficient conditions normally generates 5%–2% melts and is incapable of producing massive peraluminous felsic melts (Patiño Douce and Beard, 1995; Miller, 1985). Experimental studies have further revealed that 30% melting of metaluminous basic metaigneous rock (e. g., amphibolite) in water deficient conditions can result in the formation of calc-alkaline metaluminous tonalitic melts which are characterized by existence of melanocratic minerals (e. g., pyroxene, hornblende and biotite) and high Al, Na contents, low HREE concentrations, and strong depletion in Th, U, and LILE (Pearce, 1996). The Darongshan granites are obviously enriched in LILE, Th and U (Fig. 5a), and have high HREE concentrations (19 ppm–36 ppm; mean =

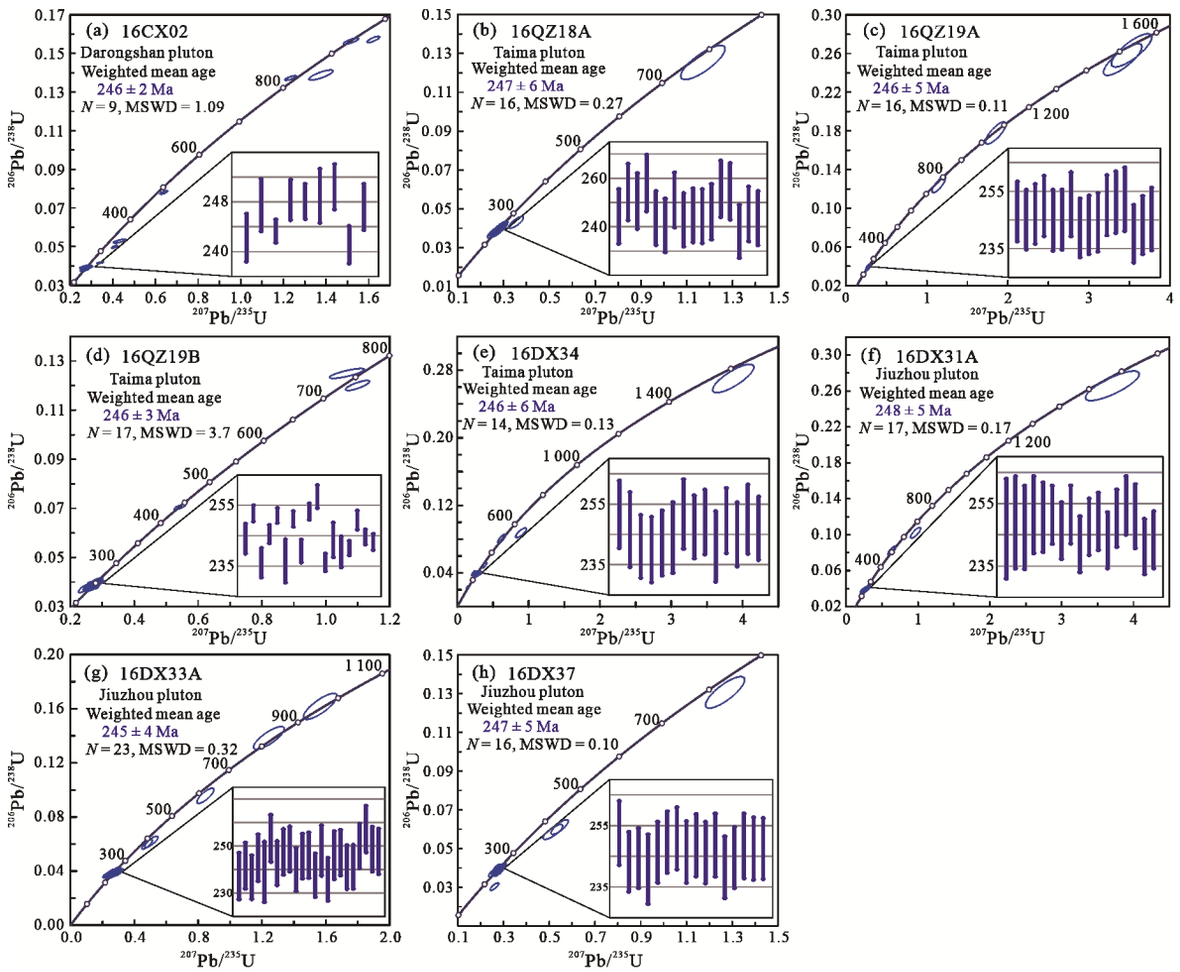

Figure 3. Zircon U-Pb concordia plots for the granite from the Qin-Fang tectonic belt.

30 ppm) and low Na_2O contents (1.95 wt.%–2.45 wt.%; average of 2.27 wt.%). These geochemical characteristics rule out that the Darongshan granites are directly originated from dehydration melting of metaluminous basic metaigneous rock (e.g., amphibolite) in the lower crustal level. Moreover, the Darongshan granites show low $\varepsilon_{Hf}(t)$ values of -14.01 – -7.75 (Table 1 and Fig. S3) which are different from those of the metabasite from the Cathaysia Block ($\varepsilon_{Hf}(t)$ = -7 – -3; Xu et al., 2005). This also suggests that the granites are not purely derived from partial melting of metabasite (e.g., amphibolite).

The Darongshan granites are characterized by enrichment in Hf isotopic compositions, low Al_2O_3/TiO_2, Rb/Sr, Rb/Ba, and $(Na_2O + K_2O)/(FeO^T + MgO + TiO_2)$ ratios, and high CaO/Na_2O ratios. This suggests that their source is similar to the melts originated from psammite source (Feng et al., 2022; Simons et al., 2016; Clemens, 2003; Miller, 1985). Field geological work shows that the Darongshan granites contain metasedimentary and quartzo-feldspathic gneissic enclaves. In addition, most of the Darongshan granite samples fall close to the calculated psammite-derived melt in the plot of Rb/Sr versus Rb/Ba (Fig. 6b). This evidence further suggests that psammitic rock is likely to be the main source of the Darongshan granites.

The results of zircon U-Pb age show that the Darongshan granites contain lots of Early Paleoproterozoic–Mesoproterozoic (2 287–1 072 Ma, Table S1) inherited zircon grains. Detrital zircon U-Pb geochronological and in-situ Hf isotopic data of the basement rocks from the Cathaysia Block also contain numerous Mesoarchean–Mesoproterozoic zircon ages (Yu et al., 2010; Xu et al., 2005). Zhou et al., (2015) reported Late Archean – Early Paleoproterozoic magmatism in the Yunkai massif and further proposed they were originated from Paleo – Mesoarchean crustal materials. The Hf isotopic data in this study show that the Darongshan granites have two-stage model ages (T_{DM2}) ranging from 1.74 to 1.43 Ga (Table 1, Fig. S3). These data indicate that the source materials (e.g., psammitic rock) of the Darongshan granites are derived from the Early Paleoproterozoic – Mesoproterozoic basement rocks. It is worth noting that the Darongshan granites have $\varepsilon_{Hf}(t)$ values ranging from -14.01 to -7.75, higher than those of the Early Paleoproterozoic – Mesoproterozoic basement rocks ($\varepsilon_{Hf}(t)$ = -20 – -16; Zhou, 2018) of the South China Block. Additionally, some of the Darongshan granite samples fall into the area of partial melts of greywacke, while others plot into the zone of partial melts of amphibolite or metabasaltic to metatonalitic source in the discrimination diagrams (Figs. 6c and 6d). All the above evidence suggests that mafic components from ancient mafic rocks and/or coeval mafic rocks are involved in the source.

Recently, a series of mafic igneous rocks were reported in the Qin-Fang tectonic belt. Xu et al. (2018) reported Early Triassic (250–248 Ma, LA-ICP-MS zircon U-Pb age) dolerites in

Table 2 Major (in wt.%) and trace elements (in ppm) for the granite from the Qin-Fang tectonic belt

Sample No.	16CX02	16RX07	16RX09	16QZ18A	16QZ19A	16QZ19B	16DX34	16DX38	16DX39	16DX31A	16DX31B	16DX31C	16DX33A	16DX33B	16DX33C	16DX37
Rock Type	Granite	Granite	Granite	Granite	Granite	Granite	Granite	Granite	Granite	Granite	Granite	Granite	Granite	Granite	Granite	Granite
Pluton	Darongshan			Taima						Jiuzhou						
SiO_2	71.60	71.28	70.95	71.76	72.98	71.31	75.02	75.08	73.87	71.18	70.75	71.08	71.28	71.20	70.82	75.91
TiO_2	0.55	0.49	0.50	0.36	0.33	0.37	0.22	0.20	0.20	0.54	0.56	0.57	0.55	0.58	0.57	0.19
Al_2O_3	13.06	13.83	13.74	14.27	14.06	14.42	13.12	13.24	13.13	12.92	13.22	13.11	13.20	13.48	13.56	12.20
$Fe_2O_3^T$	4.06	3.80	3.45	2.35	2.11	2.55	2.10	2.01	2.00	4.67	4.90	4.92	3.76	3.88	3.86	1.25
MnO	0.05	0.04	0.04	0.03	0.03	0.04	0.03	0.04	0.03	0.06	0.06	0.06	0.05	0.06	0.06	0.01
MgO	1.43	1.40	1.04	0.53	0.47	0.64	0.34	0.28	0.28	0.53	0.56	0.56	0.83	0.88	0.88	0.18
CaO	1.71	1.02	2.01	2.17	2.24	2.46	1.14	1.10	1.07	1.93	1.97	1.98	1.70	1.76	1.76	0.63
Na_2O	2.12	2.03	2.34	2.29	2.26	2.34	2.05	1.95	2.45	2.33	2.23	2.45	2.36	2.27	2.28	2.34
K_2O	3.72	3.90	4.09	4.67	4.53	4.48	4.77	4.81	4.85	4.27	4.37	4.43	4.82	4.89	4.76	5.52
P_2O_5	0.19	0.15	0.15	0.13	0.12	0.12	0.12	0.12	0.12	0.14	0.14	0.15	0.13	0.13	0.13	0.06
L.O.I	1.03	1.92	1.37	0.78	0.64	0.54	1.07	1.15	1.23	0.64	0.56	0.44	0.71	0.81	0.88	0.93
Total	99.52	99.86	99.68	99.34	99.77	99.27	99.98	99.98	99.24	99.21	99.33	99.73	99.39	99.95	99.55	99.22
Mg#	45	46	41	34	34	37	27	25	25	21	21	21	34	34	35	25
V	57	51	39	10	7	35	<5	8	8	13	18	16	56	49	43	19
Cr	40	40	20	10	10	20	10	7	6	<10	8	8	30	32	29	10
Ga	21	20	19	20	20	21	19	4.4	5.3	19	10	10	20	13	12	19
Rb	324	207	204	236	241	234	317	319	333	227	226	210	282	328	292	392
Sr	103	99	98	108	100	112	46	44	47	102	99	95	76	86	78	21
Y	26	26	36	38	39	36	56	51	55	50	46	45	47	51	47	48
Zr	242	199	205	201	179	203	126	126	145	296	252	267	320	334	321	130
Nb	14	13	12	11	10	11	9.4	10	10	14	16	15	15	19	17	9.4
Cs	12	12	9.4	7.9	11	10	12	12	12	11	11	11	18	20	19	11
Ba	694	549	533	789	802	901	251	269	269	667	717	676	656	753	702	131
La	43	38	36	45	46	47	30	32	32	64	69	66	51	60	54	26
Ce	87	77	75	91	91	96	66	67	66	109	115	110	105	117	109	57
Pr	9.7	8.7	8.5	10	10	11	7.4	7.7	7.9	15	16	15	12	13	12	6.3
Nd	37	32	31	37	37	38	27	21	22	54	44	42	42	37	34	22
Sm	7.2	6.3	6.5	7.3	7.4	7.6	6.6	7.0	7.1	10.5	11.5	11.0	8.45	10.0	9.12	5.42
Eu	1.13	1.09	1.18	1.15	1.28	1.33	0.63	0.65	0.65	1.36	1.49	1.43	1.13	1.32	1.20	0.27
Gd	6.77	5.75	6.75	7.29	7.51	7.01	7.41	6.88	6.86	10.10	10.28	9.82	8.61	8.95	8.27	6.18
Tb	0.88	0.81	0.94	1.06	1.10	1.04	1.29	1.50	1.50	1.51	1.84	1.79	1.27	1.64	1.50	1.12
Dy	5.16	5.07	5.56	6.77	7.21	6.70	9.18	9.29	9.30	9.55	10.23	9.78	8.41	9.02	8.36	7.73
Ho	0.91	0.99	1.10	1.41	1.44	1.31	1.98	2.03	1.98	1.94	2.06	1.98	1.74	1.86	1.73	1.67
Er	2.44	2.66	2.83	3.94	4.01	3.51	5.91	5.45	5.35	5.24	5.16	5.08	4.85	4.90	4.61	4.91
Tm	0.35	0.38	0.42	0.56	0.59	0.53	0.86	0.92	0.92	0.75	0.83	0.81	0.73	0.82	0.79	0.73
Yb	2.17	2.34	2.48	3.45	3.43	3.18	5.21	5.85	5.80	4.33	5.15	4.97	4.55	5.25	4.97	4.48
Lu	0.34	0.34	0.36	0.51	0.52	0.46	0.74	0.80	0.77	0.64	0.72	0.70	0.69	0.76	0.70	0.64
Hf	6.5	5.4	6.0	5.4	5.0	5.4	4.0	4.4	4.8	8.3	9.0	9.3	8.3	9.3	9.2	4.2
Ta	2.60	1.30	1.50	0.90	1.00	1.00	1.00	1.15	1.11	1.20	1.43	1.35	1.30	1.47	1.37	0.90
Th	22	19	19	26	25	26	22	25	24	28	35	34	29	34	32	29
U	6.93	7.44	5.98	5.99	6.15	5.48	7.44	8.53	7.93	4.54	5.86	5.51	6.75	8.10	7.69	4.82

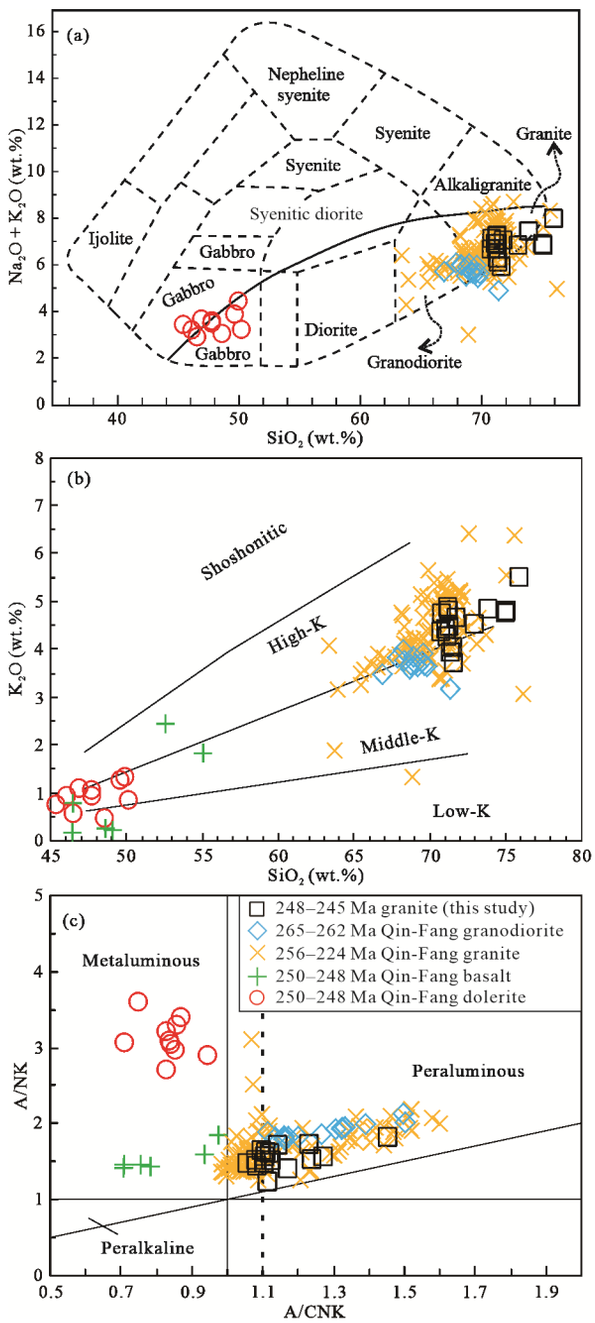

Figure 4. Plots of (a) SiO_2 versus $K_2O + Na_2O$, (b) SiO_2 versus K_2O, and (c) molecular $Al_2O_3/(CaO + Na_2O + K_2O)$ versus $Al_2O_3/(Na_2O + K_2O)$ for the granite from the Qin-Fang tectonic belt. Data for 265–262 Ma Qin-Fang granodiorite are from Li et al. (2016); the 256–224 Ma Qin-Fang granite from Zhao et al. (2012), Jiao et al. (2015); the 250–248 Ma Qin-Fang basalt and dolerite from Xu et al. (2018).

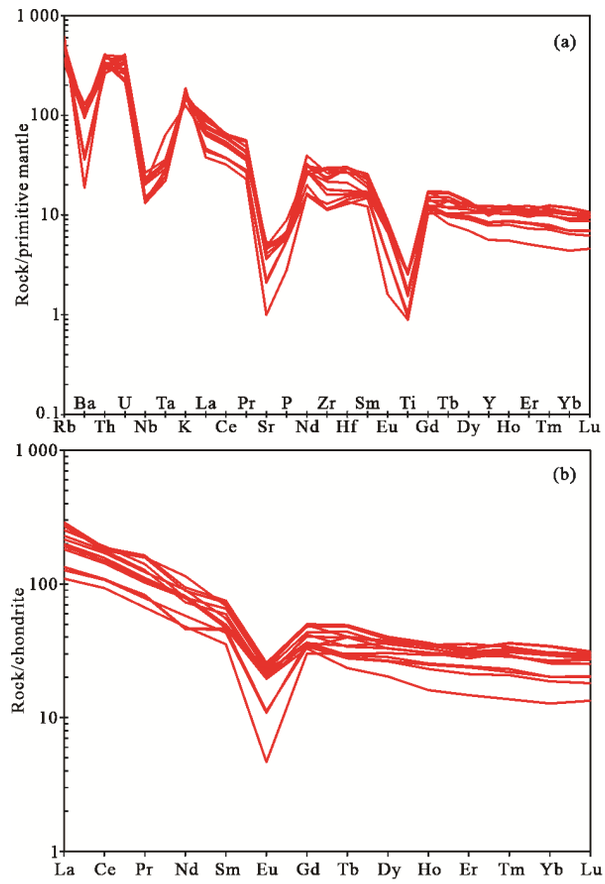

Figure 5. (a) Primitive mantle-normalized trace element spidergrams, and (b) chondrite-normalized rare earth element patterns for the granite from the Qin-Fang tectonic belt. Chondrite and primitive mantle values for normalization are from Sun and McDonough (1989).

the Darongshan area. Wu and Li (2011) reported Indosinian basalt along the Lingshan fault. Xu et al. (2015) identified 237–230 Ma (LA-ICP-MS zircon U-Pb age) gabbro-norite in the Tengxian area. Zhao et al. (2016) presented 249 ± 3 Ma (LA-ICP-MS zircon U-Pb age) hornblende gabbro along the Cenxi-Wuzhou fault. Zhao et al. (2012) reported metasedimentary granulite enclaves hosted in the Darongshan granite. These geological data show that Triassic mafic magmatism and coeval metamorphism are widely distributed in the Qin-Fang tectonic belt. The underplating of mafic magmas can provide heat needed to melt basement rocks.

Additionally, the decrease of MgO, $Fe_2O_3^T$, CaO, and TiO_2 with increasing SiO_2 (Fig. S2), together with the obvious negative Sr, Ti, and Eu anomalies (Fig. 5), indicate that fractional crystallization has played a role during magma evolution.

3.2 Tectonic Implications

Previous studies have shown that Late Permian to Early Triassic igneous rocks are widely distributed in the Jinshajiang, Ailaoshan, and Hainan Island areas (Fig. S4). The 247–246 Ma rhyolites were reported in the Jinshajiang suture zone and were regarded as representing the beginning of collision between the Indochina and Yangtze blocks (Zi et al., 2012), whereas the 234–231 Ma granitoids in the suture zone were generated in a post-collisional environment in response to the subduction of Paleo-Tethys Ocean (Zhu et al., 2011). Liu et al. (2015) obtained 252–248 Ma granites in the Ailaoshan suture zone and further proposed that convergent margin magmatism along the Jinshajiang-Ailaoshan suture zone was terminated at ca. 247 Ma. The 254–252 and 243–228 Ma granites on the Hainan Island were considered to be produced in continental arc and subsequent extensional settings in response to the subduction of Paleo-Tethyan oceanic crust (Yan et al., 2017).

Based on the above-mentioned data, the Jinshajiang-

Ailaoshan-Hainan suture zone was considered to represent a branch of the Paleo-Tethyan Ocean (Yin et al., 2023; Wang et al., 2022; Yan et al., 2017; Liu et al., 2015; Zi et al., 2012; Zhu et al., 2011; Jian et al., 2009). In this study, we propose that the Qin-Fang tectonic belt represents another branched ocean basin of the eastern Paleo-Tethys based on the following evidence. (1) The Darongshan, Taima and Jiuzhou plutons along the Qin-Fang tectonic belt have similar intrusion age of 245–248 Ma (Fig. 3). Furthermore, coeval (260–230 Ma) mafic igneous rocks (basalt, dolerite, gabbro-norite, and hornblende gabbro) have been obtained in the Qin-Fang tectonic belt (Xu et al., 2018, 2015; Zhao et al., 2016; Wu and Li, 2011; Zhang et al., 2003). The rock association and formation age in the Qin-Fang tectonic belt can be well correlated with the igneous rocks along the Jinshajiang-Ailaoshan-Hainan suture zone (Fig. S4). This indicates that the Qin-Fang tectonic belt is likely to be part of the eastern Paleo-Tethyan system. (2) The basalt, dolerite, gabbro-norite, and hornblende gabbro in the Qin-Fang tectonic belt show typical arc-related geochemical features, such as depletion of Nb and Ta (Xu et al., 2018, 2015; Zhao et al., 2016; Wu and Li, 2011). This suggests that their formation is related to arc-related magmatism. (3) Geochemical characteristics show that most of the granite samples from the Qin-Fang tectonic belt plot into the area of post-collision granite (Fig. 7). This suggests that the tectonic environment in the region was likely in a phase of post-collision. (4) Paleontological data show that radiolarian from the Devonian–Permian siliceous rocks in the Qin-Fang tectonic belt contains numerous *Holoeciscus* and *Albaillellaria* (Wang and Kuang, 1993). This indicates that they are originated from ocean. Few fora-

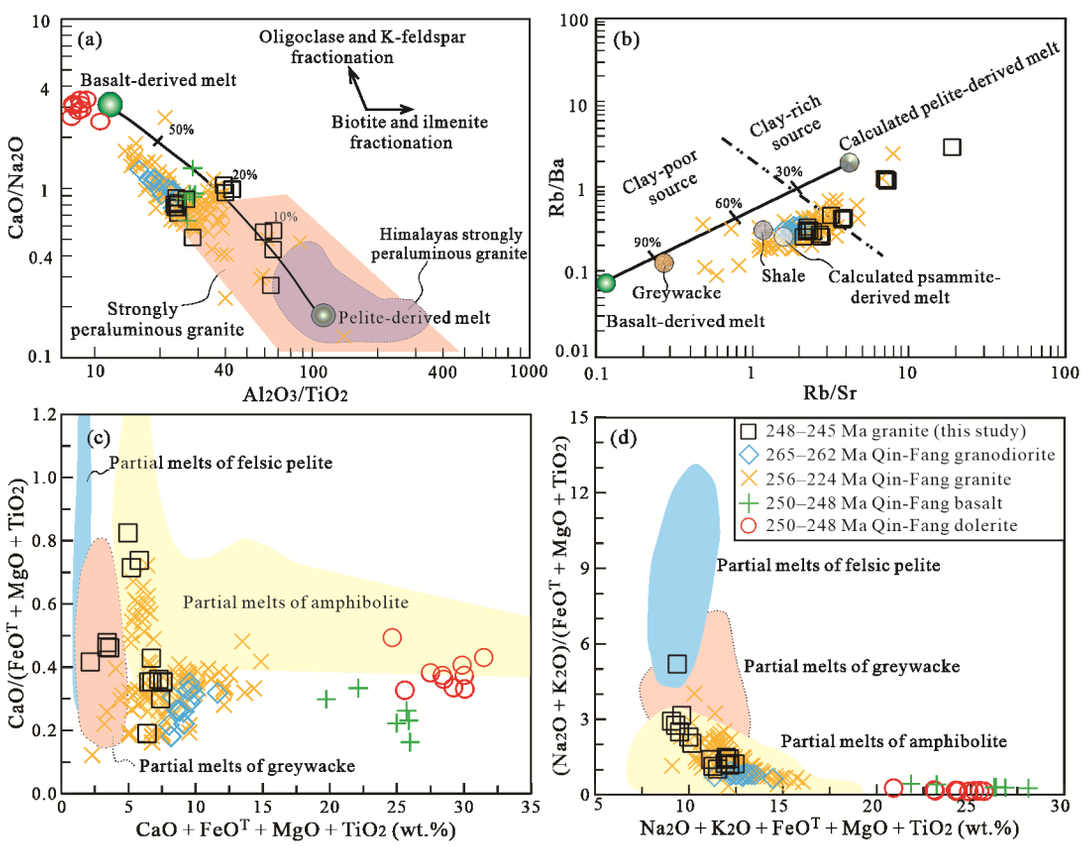

Figure 6. Plots of (a) Al_2O_3/TiO_2 versus CaO/Na_2O, (b) Rb/Sr versus Rb/Ba, (c) $CaO + FeO^T + MgO + TiO_2$ versus $CaO/(FeO^T + MgO + TiO_2)$, and (d) $Na_2O + K_2O + FeO^T + MgO + TiO_2$ versus $(Na_2O + K_2O)/(FeO^T + MgO + TiO_2)$ for the granite from the Qin-Fang tectonic belt. The symbols are as in Fig. 4.

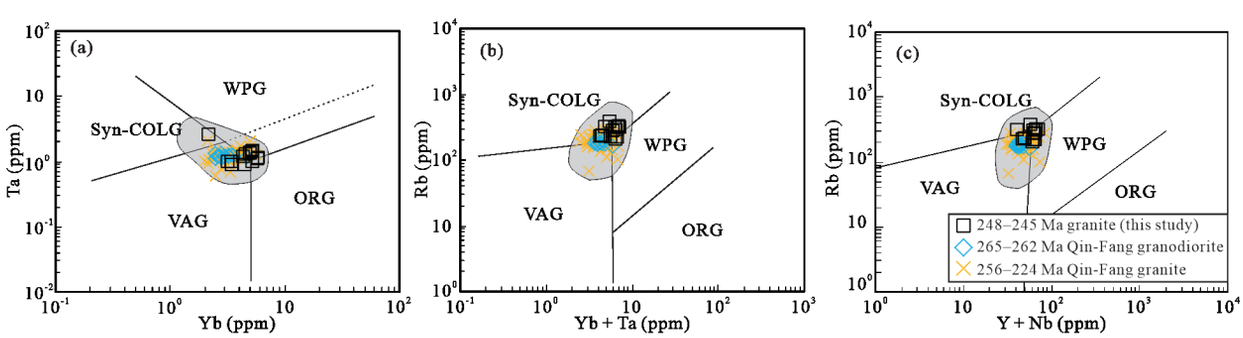

Figure 7. Plots of (a) Yb versus Ta, (b) Yb + Ta versus Rb, and (c) Y + Nb versus Rb for the granite from the Qin-Fang tectonic belt (modified from Pearce et al., 1984). WPG. Within-plate granite; Syn-COLG. syn-collision granite; VAG. volcanic arc granite; ORG. ocean-ridge granite. The symbols are as in Fig. 4.

minifera, macrofossil and coarse terrigenous detritus in the siliceous rock are distinctly different from those in the Yangtze Block which contains lots of epibenthos and fine-grained terrigenous detritus, but are generally similar to those in the Jinshajiang-Ailaoshan-Hainan suture zone (Wang and Kuang, 1993). (5) The Permian–Early Triassic sedimentary sequence in the Qin-Fang, Ailaoshan, and Hainan Island areas generally shows similar rock assemblage, i. e., silicalite and carbonatite at the bottom and sandstone and siltstone on the top. However, The Permian-Triassic strata in the Yunkai massif (SW Cathaysia Block) are missing. This indicates that different from the Yunkai Massif, the Qin-Fang, Ailaoshan, and Hainan Island areas have most likely undergone similar tectonic evolution history during the Permian–Early Triassic. (6) Detrital zircon U-Pb age and Hf isotope studies reveal that the Permian–Triassic detrital zircons in the Qin-Fang tectonic belt show a minimum age peak of 277 Ma, and most of the 277 Ma detrital zircons have negative $\varepsilon_{Hf}(t)$ (-0.43 to -19.11, our unpublished data) values. The Triassic detrital zircons in the Ailaoshan suture zone show a minimum age peak of 257 Ma and most of them have $\varepsilon_{Hf}(t)$ from -1.83 to -18.95, whereas those in the SW Yangtze Block show a minimum age peak of 270 Ma and most have positive $\varepsilon_{Hf}(t)$ (+0.15 to +9.11) (Xu, 2019). These data demonstrate that the Permian–Triassic detrital zircons in the Qin-Fang tectonic belt and Ailaoshan suture zone have similar Hf isotopic compositions, but are different from those in the SW Yangtze Block. This suggests that the Permian–Triassic detrital zircons in the Qin-Fang tectonic belt and Ailaoshan suture zone have similar source and sedimentary environment.

The above evidence indicates that the Qin-Fang tectonic

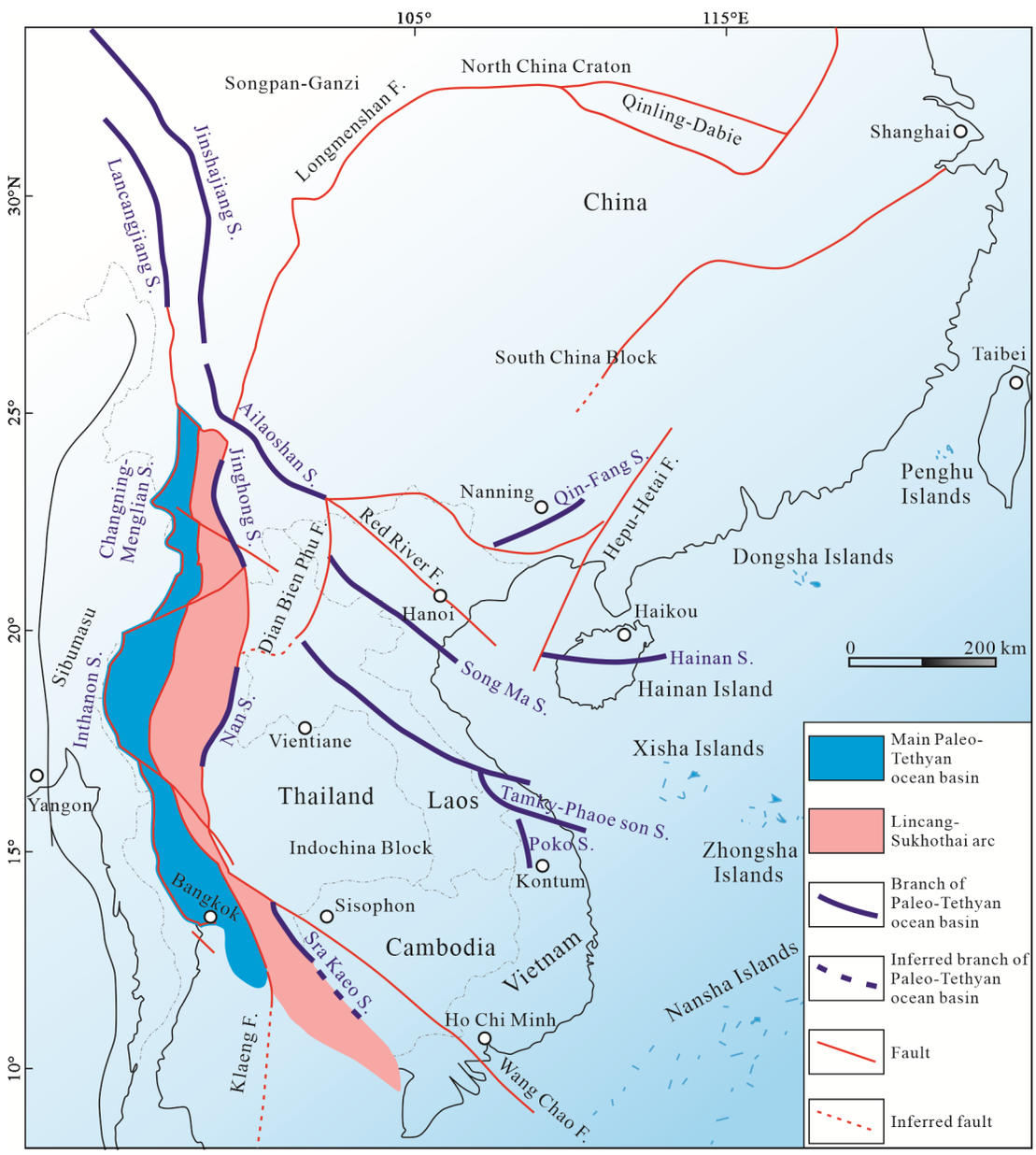

Figure 8. Schematic geotectonic map showing the main and branched Paleo-Tethyan ocean basin in SE Asia (modified after Zhao et al., 2019; Peng et al., 2013). Positions of the suture zone are synthetically compiled from Wang et al. (2022); Qian et al. (2019); Zhai et al. (2019); He et al. (2018); Liu et al. (2015); Lai et al. (2014); Peng et al. (2013); Zi et al. (2012); Jian et al. (2009); Sone and Metcalfe (2008). S. Suture; F. fault.

belt and the Jinshajiang-Ailaoshan-Hainan Island may have similar geodynamic mechanism that is related to the evolution of Paleo-Tethys during the Permian-Triassic. The evolution of the suture zones of the branched Paleo-Tethyan ocean along the Jinshajiang-Ailaoshan-Hainan Island and the Qin-Fang areas can be further summarized as follows. The Late Devonian pyroclast and deep marine radiolaria in silicalite, together with the ca. 362 Ma ophiolitic relics in the suture zones, indicate that the opening of the branch of the Paleo-Tethys ocean started in the Late Devonian (Fig. S4). Sea-floor spreading initiated in the Early Carboniferous as constrained by ca. 349 Ma ophiolitic relics and ca. 328 Ma plagiogranite (Li et al., 2018; Jian et al., 2009) and lasted till Early Permian as evidenced by a deep trough and a suite of bimodal volcanic rocks (Fig. S4; Lai et al., 2014; Trung et al., 2006). Subduction is well recorded by an arc volcanic rock belt during the Late Permian (Liu et al., 2015). Closure of the ocean and subsequent collision occurred in the early Triassic as determined by a set of collisional arc volcanic rocks and granites along the Jinshajiang-Ailaoshan-Hainan Island and the Qin-Fang suture zones (Fig. S4). Therefore, our study, combined with regional geochronological, sedimentological, and biostratigraphic data suggest that the framework of the eastern Paleo-Tethys is characterized by archipelagic ocean system, that is, in addition to the main ocean basin (e. g., the Changning-Menglian suture zone), several branched ocean basins (e. g., the Qin-Fang, the Jinshajiang-Ailaoshan-Hainan Island, and the Jinghong suture zones in South China; the Song Ma, the Tamky-Phaoe Son, and the Poko suture zones in Vietnam and Laos; the Nan and the Sra Kaeo suture zones in Thailand) of the eastern Paleo-Tethys were distributed in SE Asia (Fig. 8).

4 CONCLUSIONS

(1) A stage of Early Triassic (248 – 245 Ma) magmatism occurred in the Darongshan-Taima-Jiuzhou areas along the Qin-Fang tectonic belt.

(2) The granites were derived from psammitic rocks and contaminated a small proportion of mantle-derived materials.

(3) The Qin-Fang tectonic belt represents a branched ocean basin of the eastern Paleo-Tethys.

ACKNOWLEDGMENTS

We thank Lianhua Ma and Xiaoqian Su for their support with field work, and Linxin Meng and Yichao Ma for assistance with chemical analyses. We are grateful to the reviewers for their valuable suggestions and constructive comments on this paper. This study was financially supported by the National Natural Science Foundation of China (No. 42372102), the Guangxi Natural Science Foundation Program (Nos. 2017GXNSFAA198209 and 2022GXNSFAA035620), and the Guangxi Key R&D Program (No. AB22035045). The final publication is available at Springer via https://doi.org/10.1007/s12583-020-1111-6.

Electronic Supplementary Materials: Supplementary materials (ESM I Figs. S1–S4, ESM II Tables S1–S2) are available in the online version of this article at https://doi. org/10.1007/s12583-020-1111-6.

Conflict of Interest

The authors declare that they have no conflict of interest.

REFERENCES CITED

Allen, M. B., Song, S. G., Wang, C., et al., 2023. An Oblique Subduction Model for Closure of the Proto-Tethys and Palaeo-Tethys Oceans and Creation of the Central China Orogenic Belt. *Earth-Science Reviews*, 240: 104385. https://doi.org/10.1016/j.earscirev.2023.104385

Cai, Y. F., Liu, H. C., Feng, Z. H., et al., 2020. Neoproterozoic Active Margin of the SW South China Block: Constraints from U-Pb Ages, Sr-Nd Isotopes and Geochemical Data for the Gabbro and Granodiorite along the Ailaoshan Tectonic Belt. *Lithos*, 358/359: 105387. https://doi.org/10.1016/j.lithos.2020.105387

Cai, Y. F., Wang, Y. J., Cawood, P. A., et al., 2014. Neoproterozoic Subduction along the Ailaoshan Zone, South China: Geochronological and Geochemical Evidence from Amphibolite. *Precambrian Research*, 245: 13–28. https://doi.org/10.1016/j.precamres.2014.01.009

Champion, D. C., Bultitude, R. J., 2013. The Geochemical and Sr-Nd Isotopic Characteristics of Paleozoic Fractionated S-Types Granites of North Queensland: Implications for S-Type Granite Petrogenesis. *Lithos*, 162/163: 37–56. https://doi.org/10.1016/j.lithos.2012.11.022

Chappell, B. W., White, A. J. R., 1974. Two Contrasting Granite Types. *Pacific Geology*, 8: 173–174

Chappell, B. W., Wyborn, D., 2012. Origin of Enclaves in S-Type Granites of the Lachlan Fold Belt. *Lithos*, 154: 235 – 247. https://doi. org/10.1016/j.lithos.2012.07.012

Charoy, B., Barbey, P., 2008. Ferromagnesian Silicate Association in S-Type Granites: The Darongshan Granitic Complex (Guangxi, South China). *Bulletin Geological Society of France*, 179: 13 – 27. https://doi.10.2113/gssgfbull.179.1.13

Chen, C. H., Hsieh, P. S., Lee, C. Y., et al., 2011. Two Episodes of the Indosinian Thermal Event on the South China Block: Constraints from LA-ICPMS U-Pb Zircon and Electron Microprobe Monazite Ages of the Darongshan S-Type Granitic Suite. *Gondwana Research*, 19(4): 1008–1023. https://doi.org/10.1016/j.gr.2010.10.009

Clemens, J. D., 2003. S-Type Granitic Magmas—Petrogenetic Issues, Models and Evidence. *Earth-Science Reviews*, 61(1/2): 1 – 18. https://doi.org/10.1016/s0012-8252(02)00107-1

Deng, X. G., Chen, Z. G., Li, X. H., et al., 2004. SHRIMP U-Pb Zircon Dating of the Darongshan—Shiwandashan Granitoid Belt in Southeastern Guangxi, China. *Geological Review*, 50: 426 – 432 (in Chinese with English Abstract)

Fan, W. M., Wang, Y. J., Zhang, Y. H., et al., 2015. Paleotethyan Subduction Process Revealed from Triassic Blueschists in the Lancang Tectonic Belt of Southwest China. *Tectonophysics*, 662: 95–108. https://doi.org/10.1016/j.tecto.2014.12.021

Feng, K., Li, R. B., Pei, X. Z., et al., 2022. Zircon U-Pb Chronology, Geochemistry and Geological Significance of Late Triassic Intermediate-Acid Volcanic Rocks in Boluositai Area, East Kunlun Orogenic Belt. *Earth Science*, 47(4): 1194 – 1216. https://doi. org/10.3799/dqkx.2021.116 (in Chinese with English Abstract)

He, W. Y., Yang, L. Q., Lu, Y. J., et al., 2018. Zircon U-Pb Dating, Geochemistry and Sr-Nd-Hf-O Isotopes for the Baimaxueshan Granodiorites and Mafic Microgranulars Enclaves in the Sanjiang Orogen: Evidence for Westward Subduction of Paleo-Tethys. *Gondwana Research*, 62: 112–126. https://doi.org/10.1016/j.gr.2018.03.011

Jian, P., Liu, D. Y., Kröner, A., et al., 2009. Devonian to Permian Plate Tectonic Cycle of the Paleo-Tethys Orogen in Southwest China (II):

Insights from Zircon Ages of Ophiolites, Arc/Back-Arc Assemblages and Within-Plate Igneous Rocks and Generation of the Emeishan CFB Province. *Lithos*, 113(3/4): 767 – 784. https://doi. org/10.1016/j.lithos.2009.04.006

Jiao, S. J., Li, X. H., Huang, H. Q., et al., 2015. Metasedimentary Melting in the Formation of Charnockite: Petrological and Zircon U-Pb-Hf-O Isotope Evidence from the Darongshan S-Type Granitic Complex in Southern China. *Lithos*, 239: 217–233. https://doi.org/10.1016/j.lithos.2015.10.004

Kalsbeek, F., Jepsen, H. F., Jones, K. A., 2001. Geochemistry and Petrogenesis of S-Type Granites in the East Greenland Caledonides. *Lithos*, 57(2/3): 91–109. https://doi.org/10.1016/s0024-4937(01)00038-x

Kamei, A., 2002. Petrogenesis of Cretaceous Peraluminous Granite Suites with Low Initial Sr Isotopic Ratios, Kyushu Island, Southwest Japan Arc. *Gondwana Research*, 5(4): 813 – 822. https://doi. org/10.1016/s1342-937x(05)70915-1

Lai, C. K., Meffre, S., Crawford, A. J., et al., 2014. The Western Ailaoshan Volcanic Belts and Their SE Asia Connection: A New Tectonic Model for the Eastern Indochina Block. *Gondwana Research*, 26(1): 52 – 74. https://doi.org/10.1016/j.gr.2013.03.003

Li, S. B., He, H. Y., Qian, X., et al., 2018. Carboniferous Arc Setting in Central Hainan: Geochronological and Geochemical Evidences on the Andesitic and Dacitic Rocks. *Journal of Earth Science*, 29(2): 265 – 279. https://doi: 10.1007/s12583-017-0936-0

Li, Y. J., Wei, J. H., Santosh, M., et al., 2016. Geochronology and Petrogenesis of Middle Permian S-Type Granitoid in Southeastern Guangxi Province, South China: Implications for Closure of the Eastern Paleo-Tethys. *Tectonophysics*, 682: 1 – 16. https://doi. org/10.1016/j.tecto.2016.05.048

Liu, F., Lin, W., Wang, Y., et al., 2023. Heterogeneity of the Ailaoshan-Song Ma Ophiolitic Mélange and Its Palaeogeographic Implications for the Evolution of Eastern Palaeo-Tethys. *Tectonophysics*, 858: 229848. https://doi.org/10.1016/j.tecto.2023.229848

Liu, H. C., Wang, Y. J., Cawood, P. A., et al., 2015. Record of Tethyan Ocean Closure and Indosinian Collision along the Ailaoshan Suture Zone (SW China). *Gondwana Research*, 27(3): 1292–1306. https://doi.org/10.1016/j.gr.2013.12.013

Ma, Y. C., Cai, Y. F., Ma, L. Y., et al., 2021. Genesis of Neoproterozoic Amphibolite in Diancangshan, West Yunnan: Evidence from Zircon U-Pb Age and Whole-Rock Geochemistry. *Earth Science*, 46(8): 2860–2872. https://doi.org/10.3799/dqkx.2020.288 (in Chinese with English Abstract)

Metcalfe, I., 1996. Gondwanaland Dispersion, Asian Accretion and Evolution of Eastern Tethys. *Australian Journal of Earth Sciences*, 43(6): 605–623. https://doi.org/10.1080/08120099608728282

Miller, C. F., 1985. Are Strongly Peraluminous Magmas Derived from Pelitic Sedimentary Sources? *The Journal of Geology*, 93(6): 673–689. https://doi.org/10.1086/628995

Patiño Douce, A. E., Beard, J. S., 1995. Dehydration-Melting of Biotite Gneiss and Quartz Amphibolite from 3 to 15 Kbar. *Journal of Petrology*, 36(3): 707–738. https://doi.org/10.1093/petrology/36.3.707

Pearce, J. A., 1996. Sources and Settings of Granitic Rocks. *Episodes*, 19(4): 120–125. https://doi.org/10.18814/epiiugs/1996/v19i4/005

Pearce, J. A., Harris, N. B. W., Tindle, A. G., 1984. Trace Element Discrimination Diagrams for the Tectonic Interpretation of Granitic Rocks. *Journal of Petrology*, 25(4): 956–983. https://doi. org/10.1093/petrology/25.4.956

Peng, T. P., Wilde, S. A., Wang, Y. J., et al., 2013. Mid-Triassic Felsic Igneous Rocks from the Southern Lancangjiang Zone, SW China: Petrogenesis and Implications for the Evolution of Paleo-Tethys. *Lithos*, 168/169: 15–32. https://doi.org/10.1016/j.lithos.2013.01.015

Qian, X., Wang, Y. J., Zhang, Y. Z., et al., 2019. Petrogenesis of Permian-Triassic Felsic Igneous Rocks along the Truong Son Zone in Northern Laos and Their Paleotethyan Assembly. *Lithos*, 328/329: 101 – 114. https://doi.org/10.1016/j.lithos.2019.01.006

Qin, X. F., Wang, Z. Q., Cao, J., et al., 2013. Petrogenesis of Early Indosinian Granites from the Southwestern Segment of Qinfang Tectonic Belt, Southern Guangxi: Constraints from Zircon U-Pb Chronology and Geochemistry. *Journal of Jilin University* (*Earth Science Edition*), 43: 1471–1488 (in Chinese with English Abstract)

Qiu, X., Wang, Y. J., Qian, X., et al., 2021. Detrital Zircon U-Pb Geochronology and Geochemical Characteristics of Permian Sandstones in NW Laos and Its Tectonic Implications. *Earth Science*, 46(11): 3910–3925. https://doi.org/10.3799/dqkx.2020.379 (in Chinese with English Abstract)

Şengör, A. M. C., 1979. Mid-Mesozoic Closure of Permo-Triassic Tethys and Its Implications. *Nature*, 279(5714): 590 – 593. https://doi. org/10.1038/279590a0

Shi, M. F., Wu, Z. B., Liu, S. S., et al., 2019. Geochronology and Petrochemistry of Volcanic Rocks in the Xaignabouli Area, NW Laos. *Journal of Earth Science*, 30(1): 37 – 51. https://doi: 10.1007/s12583-018-0863-8

Simons, B., Shail, R. K., Andersen, J. C. Ø., 2016. The Petrogenesis of the Early Permian Variscan Granites of the Cornubian Batholith: Lower Plate Post-Collisional Peraluminous Magmatism in the Rhenohercynian Zone of SW England. *Lithos*, 260: 76–94. https://doi.org/10.1016/j.lithos.2016.05.010

Sone, M., Metcalfe, I., 2008. Parallel Tethyan Sutures in Mainland Southeast Asia: New Insights for Palaeo-Tethys Closure and Implications for the Indosinian Orogeny. *Comptes Rendus Geoscience*, 340(2/3): 166–179. https://doi.org/10.1016/j.crte.2007.09.008

Sun, S. S., McDonough, W. F., 1989. Chemical and Isotopic Systematics of Oceanic Basalts: Implications for Mantle Composition and Processes. *Geological Society*, *London*, *Special Publications*, 42(1): 313 – 345. https://doi.org/10.1144/gsl.sp.1989.042.01.19

Sylvester, P. J., 1998. Post-Collisional Strongly Peraluminous Granites. *Lithos*, 45(1/2/3/4): 29 – 44. https://doi. org/10.1016/s0024-4937(98)00024-3

Trung, N. M., Tsujimori, T., Itaya, T., 2006. Honvang Serpentinite Body of the Song Ma Fault Zone, Northern Vietnam: A Remnant of Oceanic Lithosphere within the Indochina-South China Suture. *Gondwana Research*, 9(1/2): 225–230. https://doi.org/10.1016/j.gr.2005.06.012

Wang, F., Liu, F. L., Schertl, H. P., et al., 2019. Paleo-Tethyan Tectonic Evolution of Lancangjiang Metamorphic Complex: Evidence from SHRIMP U-Pb Zircon Dating and $^{40}Ar/^{39}Ar$ Isotope Geochronology of Blueschists in Xiaoheijiang-Xiayun Area, Southeastern Tibetan Plateau. *Gondwana Research*, 65: 142 – 155. https://doi. org/10.1016/j.gr.2018.08.007

Wang, Y., Lin, W., Faure, M., et al., 2022. Correlation among the Ailaoshan-Song Ma-Song Chay Orogenic Belts and Implications for the Evolution of the Eastern Paleo-Tethys Ocean. *Tectonophysics*, 843: 229618. https://doi.org/10.1016/j.tecto.2022.229618

Wang, Y. J., Kuang, G. D., 1993. Early Carboniferous Radiolarians from Qinzhou, Southeastern Guangxi. *Acta Micropalaeontologica Sinica*, 10: 275–287 (in Chinese with English Abstract)

Wu, G. Y., Li, Y. J., 2011. The Mashan Indosinian Oceanic Island Basalt Outcropping along the Lingshan Fracture in Southeast Guangxi and Its

Tectonic Implications. *Geoscience*, 25: 682 – 689 (in Chinese with English Abstract)

Xu, X. S., O'Reilly, S. Y., Griffin, W. L., et al., 2005. Relict Proterozoic Basement in the Nanling Mountains (SE China) and Its Tectonothermal Overprinting. *Tectonics*, 24(2): TC2003. https://doi.org/10.1029/2004tc001652

Xu, H., Huang, B. C., Ni, Z. X., et al., 2015. LA-ICP-MS Zircon U-Pb Ages, Petrogeochemistry and Tectonic Significance of the Indosinian Basic Intrusive Rocks in the Tengxian Region, Southeastern Guangxi. *Sedimentary Geology and Tethyan Geology*, 35: 76 – 87 (in Chinese with English Abstract)

Xu, J., 2019. Subduction and Closure of the Paleotethys Ailaoshan Ocean: Constraints from Sedimentation and Magmatism: [Dissertation]. Guangzhou Institute of Geochemistry, Chinese Academy of Sciences, Guangzhou (in Chinese with English Abstract)

Xu, W. C., Luo, B. J., Xu, Y. J., et al., 2018. Geochronology, Geochemistry, and Petrogenesis of Late Permian to Early Triassic Mafic Rocks from Darongshan, South China: Implications for Ultrahigh-Temperature Metamorphism and S-Type Granite Generation. *Lithos*, 308/309: 168–180. https://doi.org/10.1016/j.lithos.2018.03.004

Yan, Q. S., Metcalfe, I., Shi, X. F., 2017. U-Pb Isotope Geochronology and Geochemistry of Granites from Hainan Island (Northern South China Sea Margin): Constraints on Late Paleozoic-Mesozoic Tectonic Evolution. *Gondwana Research*, 49: 333–349. https://doi.org/10.1016/j.gr.2017.06.007

Yang, L., Yuan, W. M., Zhu, X. Y., et al., 2019. Late Triassic-Cenozoic Thermochronology in the Southern Sanjiang Tethys, SW China, New Insights from Zircon Fission Track Analysis. *Journal of Earth Science*, 30(5): 996–1004. https://doi: 10.1007/s12583-019-1014-6

Yin, S. P., Zhang, H. R., Bian, Y. K., 2023. Petrogenesis of Middle Triassic Andesitic Rocks in the Weixi Area, Southwest China: Implications for the Tectonic Evolution of the Paleo-Tethys. *Lithos*, 450/451: 107194. https://doi.org/10.1016/j.lithos.2023.107194

Yu, J. H., O'Reilly, S. Y., Wang, L. J., et al., 2010. Components and Episodic Growth of Precambrian Crust in the Cathaysia Block, South China: Evidence from U-Pb Ages and Hf Isotopes of Zircons in Neoproterozoic Sediments. *Precambrian Research*, 181(1/2/3/4): 97–114. https://doi.org/10.1016/j.precamres.2010.05.016

Zhai, Q. G., Chung, S. L., Tang, Y., et al., 2019. Late Carboniferous Ophiolites from the Southern Lancangjiang Belt, SW China: Implication for the Arc-Back-Arc System in the Eastern Paleo-Tethys. *Lithos*, 344/345: 134–146. https://doi.org/10.1016/j.lithos.2019.06.020

Zhang, B. Y., Zhang, H. X., Zhao, Z. H., et al., 2003. Permian Island-Arc Basalt in West Guangdong and East Guangxi Tectonic Belt, South China: Implications for the Paleotethys. *Journal of Nanjing University* (*Natural Sciences*), 39: 46–54 (in Chinese with English Abstract)

Zhao, G. C., Cawood, P. A., 2012. Precambrian Geology of China. *Precambrian Research*, 222/223: 13 – 54. https://doi. org/10.1016/j.precamres.2012.09.017

Zhao, G. Y., Qin, X. F., Wang, Z. Q., et al., 2016. Geochronology, Geochemistry and Geological Significance of Gabbros from Xindi-Anping Area, Southeastern Guangxi. *Acta Petrologica et Mineralogica*, 35: 791–803 (in Chinese with English Abstract)

Zhao, L., Guo, F., Fan, W. M., et al., 2012. Origin of the Granulite Enclaves in Indo-Sinian Peraluminous Granites, South China and Its Implication for Crustal Anatexis. *Lithos*, 150: 209 – 226. https://doi. org/10.1016/j.lithos.2012.02.015

Zhao, T. Y., Algeo, T. J., Feng, Q. L., et al., 2019. Tracing the Provenance of Volcanic Ash in Permian-Triassic Boundary Strata, South China: Constraints from Inherited and Syn-Depositional Magmatic Zircons. *Palaeogeography*, *Palaeoclimatology*, *Palaeoecology*, 516: 190 – 202. https://doi.org/10.1016/j.palaeo.2018.12.002

Zhao, Y. S., Zhou, Y., Xu, C., et al., 2023. Geochemical Characteristics and Rare Earth Metallogenic Indication of Yanshanian Granite in Southeast Guangxi. *Chinese Journal of Geology*, 58(3): 890 – 909 (in Chinese with English Abstract)

Zhong, D. L., 1998. Paleotethysides in Western Yunnan and Sichuan, China. Science Press, Beijing. 9–215 (in Chinese with English Abstract)

Zhou, G. Y., 2018. The Nature of Late Archean to Paleoproterozoic Basement in the Northern Yangtze and Its Geological Implication: [Dissertation]. China University of Geosciences, Wuhan (in Chinese with English Abstract)

Zhou, Y., Liang, X. Q., Liang, X. R., et al., 2015. U-Pb Geochronology and Hf-Isotopes on Detrital Zircons of Lower Paleozoic Strata from Hainan Island: New Clues for the Early Crustal Evolution of Southeastern South China. *Gondwana Research*, 27(4): 1586 – 1598. https://doi.org/10.1016/j.gr.2014.01.015

Zhu, J. J., Hu, R. Z., Bi, X. W., et al., 2011. Zircon U-Pb Ages, Hf-O Isotopes and Whole-Rock Sr-Nd-Pb Isotopic Geochemistry of Granitoids in the Jinshajiang Suture Zone, SW China: Constraints on Petrogenesis and Tectonic Evolution of the Paleo-Tethys Ocean. *Lithos*, 126(3/4): 248–264. https://doi.org/10.1016/j.lithos.2011.07.003

Zi, J. W., Cawood, P. A., Fan, W. M., et al., 2012. Generation of Early Indosinian Enriched Mantle-Derived Granitoid Pluton in the Sanjiang Orogen (SW China) in Response to Closure of the Paleo-Tethys. *Lithos*, 140/141: 166–182. https://doi.org/10.1016/j.lithos.2012.02.006